Bae *et al. Micro and Nano Systems Letters* (2022) 10:20
https://doi.org/10.1186/s40486-022-00163-6

Micro and Nano Systems Letters

LETTER Open Access

Effect of channel height on the critical particle diameter in a deterministic lateral device

Jae Hyun Bae[1], Alexander Zhbanov[1] and Sung Yang[1,2*]

Abstract

The separation of biological cells or microorganisms in a liquid based on their size by deterministic lateral displacement is widely used in laboratories. The analytical equation for the critical diameter is derived under the assumption that flow between two posts is better described by flow in a rectangular tube than between parallel plates. The height position of the particle is an additional parameter that affects the critical diameter. Preliminary experiments were carried out on the separation of particles in deep and shallow microchannels. This study shows that the critical diameter is not a constant value for a given design but is different on each plane parallel to the top and bottom of the channel. The theoretical model was used to analyze experimental data on the separation of particles larger than 4.2 μm from particles ranging in size from 2.5 to 7.9 μm.

Keywords: Microfluidics, Deterministic lateral displacement, Particle separation, Critical particle diameter

Introduction

Separation of particles by deterministic lateral displacement (DLD) is based on the movement of liquid in a rectilinear microchannel of a rectangular cross-section [1, 2]. The width of this flat microchannel significantly exceeds its height. On average, the liquid moves inside the channel parallel to its walls. At the same time, the microfabricated post arrays provide separation of particles according to their size. The top view of the middle part of the microchannel and the scheme of experimental device are shown in Fig. 1. On a large scale, the liquid moves from top to bottom parallel to the far walls. On a detailed scale, the liquid follows the "zigzag" mode formed by the streamlines (see Fig. 1A). Small particles are involved in this zigzag mode and move straight down on average. Large particles jump from one post to another and displace to the right in the "bump" or "displacement" mode. Here and below, it is assumed that each under the row of posts is shifted to the right by a row shift fraction relative to the upper row. Thus, small particles can be directed to the left, and large particles to the right (see Fig. 1B). The separation into small and large particles is determined by the critical diameter, which depends only on the micropost array geometry. Inglis et al. [2] derived an equation for the critical diameter. The derivation of the equation is based on two assumptions: firstly, the height of the microchannel is much greater than the gap between the posts or even if the posts are infinitely high, and secondly, the flow in the gap between two posts is similar to the flow between two parallel plates. Based on these assumptions, the division into small and large particles should be mathematically rigorous.

Beech [3] and Holm [4] found through 3D finite element modeling that channel height affects the flow profile and, therefore the critical diameter.

Their results for the median plane between the top and bottom of the channel show that the critical diameter increases with increasing channel height. The variation

*Correspondence: syang@gist.ac.kr
[1] School of Mechanical Engineering, Gwangju Institute of Science and Technology (GIST), Gwangju 61005, Republic of Korea
Full list of author information is available at the end of the article

© The Author(s) 2022. **Open Access** This article is licensed under a Creative Commons Attribution 4.0 International License, which permits use, sharing, adaptation, distribution and reproduction in any medium or format, as long as you give appropriate credit to the original author(s) and the source, provide a link to the Creative Commons licence, and indicate if changes were made. The images or other third party material in this article are included in the article's Creative Commons licence, unless indicated otherwise in a credit line to the material. If material is not included in the article's Creative Commons licence and your intended use is not permitted by statutory regulation or exceeds the permitted use, you will need to obtain permission directly from the copyright holder. To view a copy of this licence, visit http://creativecommons.org/licenses/by/4.0/.

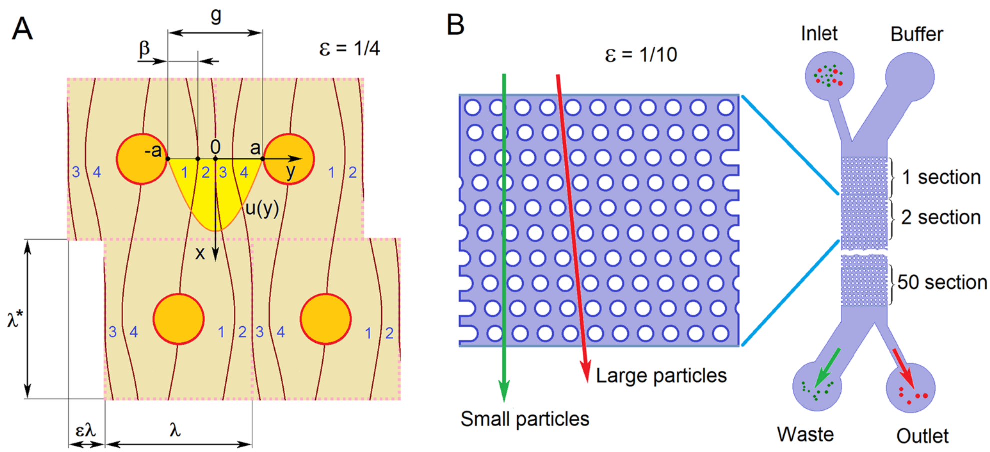

Fig. 1 Deterministic lateral displacement arrays. **A** Top view of the middle section of a typical sorting device. The pattern is laid out with rectangular mosaic tiles of size $\lambda \times \lambda^{*}$. **B** Scheme of the experimental device for the separation of large particles

of the critical diameter on other planes other than the median has not been studied.

Expert opinions on fundamental, practical, and commercial issues with DLD have been described in many reviews (see, for example, refs. [5–7]).

In practical devices, the separation efficiency is greatly reduced, so that small particles can enter the right outlet to large particles and vice versa. Published studies mention several reasons for the decrease in efficiency: clogging of the device with comparable sizes between the gap and beads, a high bead concentration, and the influence of boundaries where the periodicity of the post array is violated [2, 8]. The effects of Brownian motion and diffusion can also make it difficult to separate submicron sized beads. It can be assumed that the channel height also affects the separation efficiency.

This work aims to study the influence of the microchannel height on the critical diameter and particle separation efficiency by deterministic lateral displacement.

Theoretical analysis

The top view of the circular post array is shown in Fig. 1. The flow is caused by a pressure difference and moves down in this figure. The structure is periodical. The horizontal period is λ and the vertical period is λ^{*}. For practical reasons, the periods are usually chosen approximately equal so that $\lambda \approx \lambda^{*}$. If $\lambda < \lambda^{*}$, then the microfluidic device will be unreasonably long. In the case $\lambda > \lambda^{*}$, a big particle can get stuck between the rows. Mosaic tiles $\lambda \times \lambda^{*}$ are laid out in such a way that each subsequent row is shifted to the right by $\varepsilon\lambda$ relative to the previous one, using the row shift fraction, ε. If the value $n = 1/\varepsilon$ is a whole number, then the structure will repeat every n row. Figure 1 shows the case for $n = 4$.

The fluid is incompressible, and the flow at a long distance is limited to the right and left by non-deforming vertical bounding walls. Thus, the average flow velocity is directed strictly downward. The left and right bounding walls violate the ideal periodic structure, which leads to aberrant fluid flow near the boundaries. Inglis [8] shows how to eliminate this problem by modifying the boundary interface. However, disturbances near the boundaries have very little effect on the flow in the middle part of the microfluidic device shown in Fig. 1. Inglis et al. [2] assumed a parabolic velocity profile at the narrowest part of the flow between the two posts.

According to the theory of fluid mechanics, a parabolic velocity profile arises between two infinite parallel plates, which is described by the Hagen-Poiseuille equation. This equation, apparently, is sufficiently accurate for

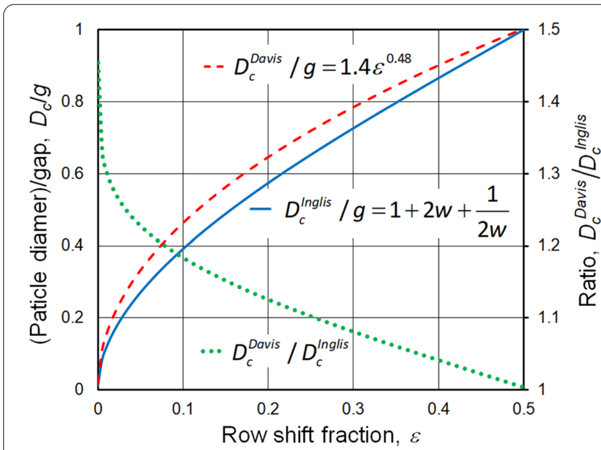

Fig. 2 Theoretical and empirical points of the particle diameter divided by the gap, versus the row shift fraction, ε (primary axis); the ratio between theoretical and empirical critical diameters (secondary axis)

a two-dimensional model of flow in microfluidic devices, which has been confirmed by many numerical calculations. In particular, Al-Fandi et al. [9] showed that the flow approaches a parabola not only between cylindrical posts but also between rhomboid and airfoil posts.

The narrowest part of the flow, the so-called gap g ($g=2a$), and the parabolic velocity profile $u(y)$ are shown in Fig. 1. The coordinate system is chosen so that the x-axis is co-directed with the flow (vertically down) and the y-axis is perpendicular (horizontally to the right).

Total flow flux through the gap g can be divided into 1,2, …, and n flow streams, as described by Huang et al. [1] and Inglis et al. [2]. In the subsequent row, the first stream bypasses the post, stream 2 becomes 1, stream 3 becomes 2, and so on (see Fig. 1). The stream numbering order is restored after passing through n rows of posts. Therefore, each stream must carry an equal fluid flux. Based on these considerations, Huang et al. [1] and Inglis et al. [2] proved that if the radius of a particle is less than the width of the first streamline β, then it will follow the zigzag mode. If the particle radius exceeds the width of the first streamline β, it will travel in the bump mode. This makes it possible to determine the critical particle diameter D_c: $D_c=2\beta$. The equivalence of fluid flow in each streamline is expressed by the following equation:

$$\int_{-a}^{-a+\beta} u(y)dy = \varepsilon \int_{-a}^{a} u(y)dy \tag{1}$$

Using the parabolic Poiseuille flow velocity profile, Inglis et al. [2] solved Eq. (1) for β and found the critical diameter (Inglis diameter):

$$D_c^{Inglis} = 2\beta_{Inglis} = g\left(1 + 2w + \frac{1}{2w}\right) = 2a\left(1 + 2w + \frac{1}{2w}\right) \tag{2}$$

where $w = \left[\frac{1}{8} - \frac{\varepsilon}{4} + \sqrt{\frac{\varepsilon}{16}(\varepsilon - 1)}\right]^{(1/3)} \left(-\frac{1}{2} - \mathrm{j}\frac{\sqrt{3}}{2}\right)$ and j is the imaginary unit j = $\sqrt{-1}$.

Equation (2) is valid for flow through an array of infinitely tall posts. The fraction $D_c^{Inglish}/g$ from Eq. (2) is shown by the blue solid line in Fig. 2. This model almost predicts the particle separation into the zigzag and bumping mode but gives an underestimated critical diameter.

Davis [10] tested the particle separation in many devices with different row shift fractions and gap sizes and devised the following empirical formula for critical diameter (Davis diameter):

$$D_c^{Davis} = 1.4g\varepsilon^{0.48} \tag{3}$$

The fraction D_c^{Davis}/g from Eq. (3) is plotted as the red dashed line in Fig. 2, which also shows the ratio D_c^{Davis}/D_c^{Inglis} by the green dotted line.

In reality, the DLD microfluidic device has a limited space between the top and bottom of the channel (see Fig. 3). It can be assumed that the flow between two posts will be described by the flow in an infinite rectangular pipe.

To consider such a flow, it is convenient to place the origin at the center of a rectangle with the range of sizes $-\mathrm{a} \le \mathrm{y} \le \mathrm{a}, -\mathrm{b} \le \mathrm{z} \le \mathrm{b}$.

The analytical solution of the Poiseuille flow in the rectangular duct is expressed as follows [11, 12]:

$$u(y,z) = \frac{16a^2}{\mu\pi^3}\left(-\frac{dp}{dx}\right)\sum_{i=1,3,5....}^{\infty}(-1)^{(i-1)/2} \left[1 - \frac{\cosh\left(i\pi z/2a\right)}{\cosh\left(i\pi b/2a\right)}\right]\frac{\cos\left(i\pi y/2a\right)}{i^3} \tag{4}$$

where μ is the dynamic viscosity and p is the hydrostatic pressure.

Figure 3 shows the velocity profiles in different planes between the top and bottom of the channel and color cross-sectional velocity maps for a to b aspect ratios of 1/2 and 1/4. The critical diameters differ at different plane levels, where $z=$const.

In the limiting case, when the channel height b tends to infinity, Eq. (2) gives a parabolic velocity profile for the Poiseuille flow between two parallel plates.

The equation for the width of the first streamline at a certain level is similar to Eq. (1):

$$\int_{-a}^{-a+\beta} u(y,z=const)dy = \varepsilon\int_{-a}^{a} u(y,z=const)dy \tag{5}$$

To compose Eq. (5), it is necessary to take the integrals of $\cos(i\pi y/2a)$:

$$\int_{-a}^{-a+\beta}\cos\left(i\pi y/2a\right)dy = \left.\frac{2a\sin\left(i\pi y/2a\right)}{i\pi}\right|_{-a}^{-a+\beta} = \frac{2a[\sin\left(i\pi(-a+\beta)/2a\right) + \sin\left(i\pi/2\right)]}{i\pi}$$

and

$$\int_{-a}^{a}\cos\left(i\pi y/2a\right)dy = \left.\frac{2a\sin\left(i\pi y/2a\right)}{i\pi}\right|_{-a}^{a} = \frac{4a\sin\left(i\pi/2\right)}{i\pi}$$

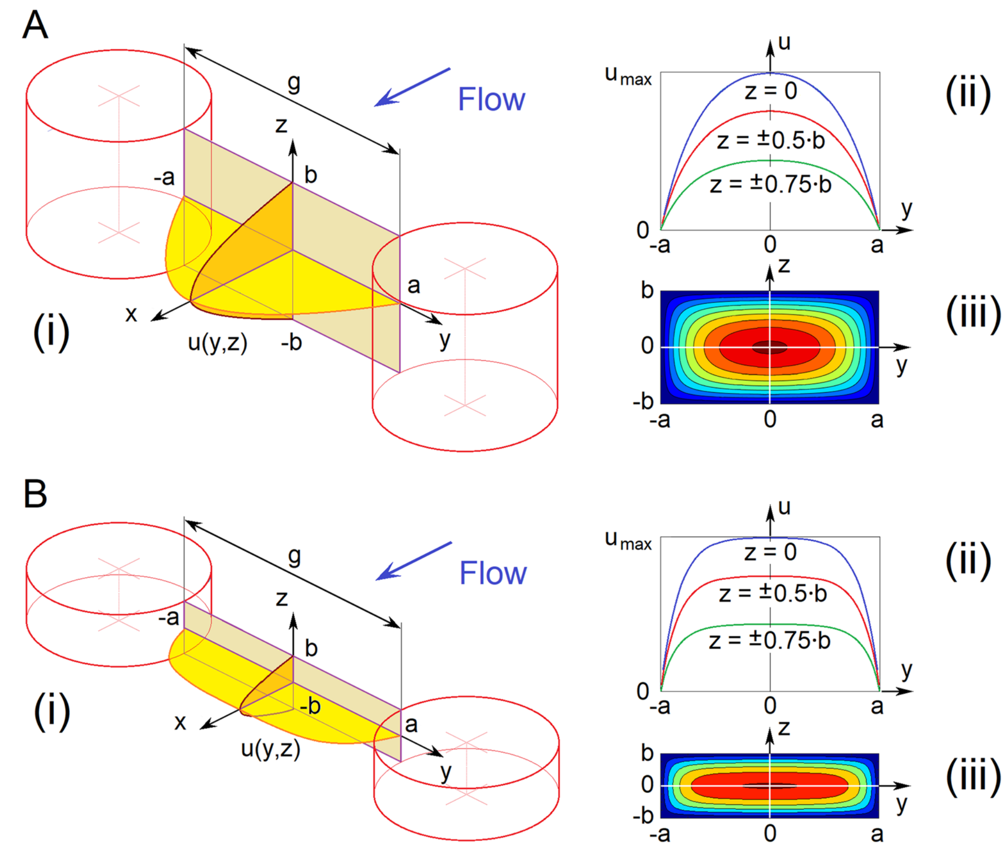

Fig. 3 Microfluidic channel height effect on the velocity profile. Height-to-width aspect ratio a/b is 1/2 (**A**) and 1/4 (**B**). (i) Flow between two posts is modeled as laminar flow in a rectangular channel. (ii) Velocity profile in different planes $z=0, \pm0.5b$, and $\pm0.75b$. (iii) Color map of the laminar flow through the rectangular pipe

After substitutions and simplification, the equation for the width β takes the form:

$$\sum_{i=1,3,5....}^{\infty}(-1)^{(i-1)/2}\frac{1}{i^4}\left[1-\frac{\cosh\left(i\pi z/2a\right)}{\cosh\left(i\pi b/2a\right)}\right]\left[\sin\left(\frac{i\pi(-a+\beta)}{2a}\right)+\sin\left(\frac{i\pi}{2}\right)-2\varepsilon\sin\left(\frac{i\pi}{2}\right)\right]=0 \quad (6)$$

In this study, Eq. (6) was solved numerically.

Variability of critical diameter

Figure 4A and C show the comparison of analytical approximation for the critical diameter of particles with the numerical solution of Eq. (6) where the velocity profiles were calculated using Eq. (4). For comparison, the following geometric parameters of the idealized device model were chosen. The gap between the posts is $g=10$ μm, and, accordingly, half of the channel width is $a=g/2=5$ μm. The row shift fraction is $\varepsilon=0.1$. The height of the deep and shallow channels is 50 and 10 μm, respectively. Thus, the aspect ratio of height to width a/b is 1/5 (Fig. 4A) and 1/1 (Fig. 4C). Additionally, Fig. 4A and C show the critical diameter calculated by Eq. (2) as a reference point.

For the selected parameters of the microfluidic device, the difference between the maximum and minimum critical diameter is about 0.5 μm. The maximum critical diameter in a shallow channel is smaller than in a deep one. If the channel height tends to infinity, then the critical diameter does not depend on the particle position and tends to the value described by Eq. (2). Thus, the separation efficiency increases as the channel height increases. Comparison of Fig. 3B and D shows that the separation boundary between small and large particles is sharer for a deeper channel.

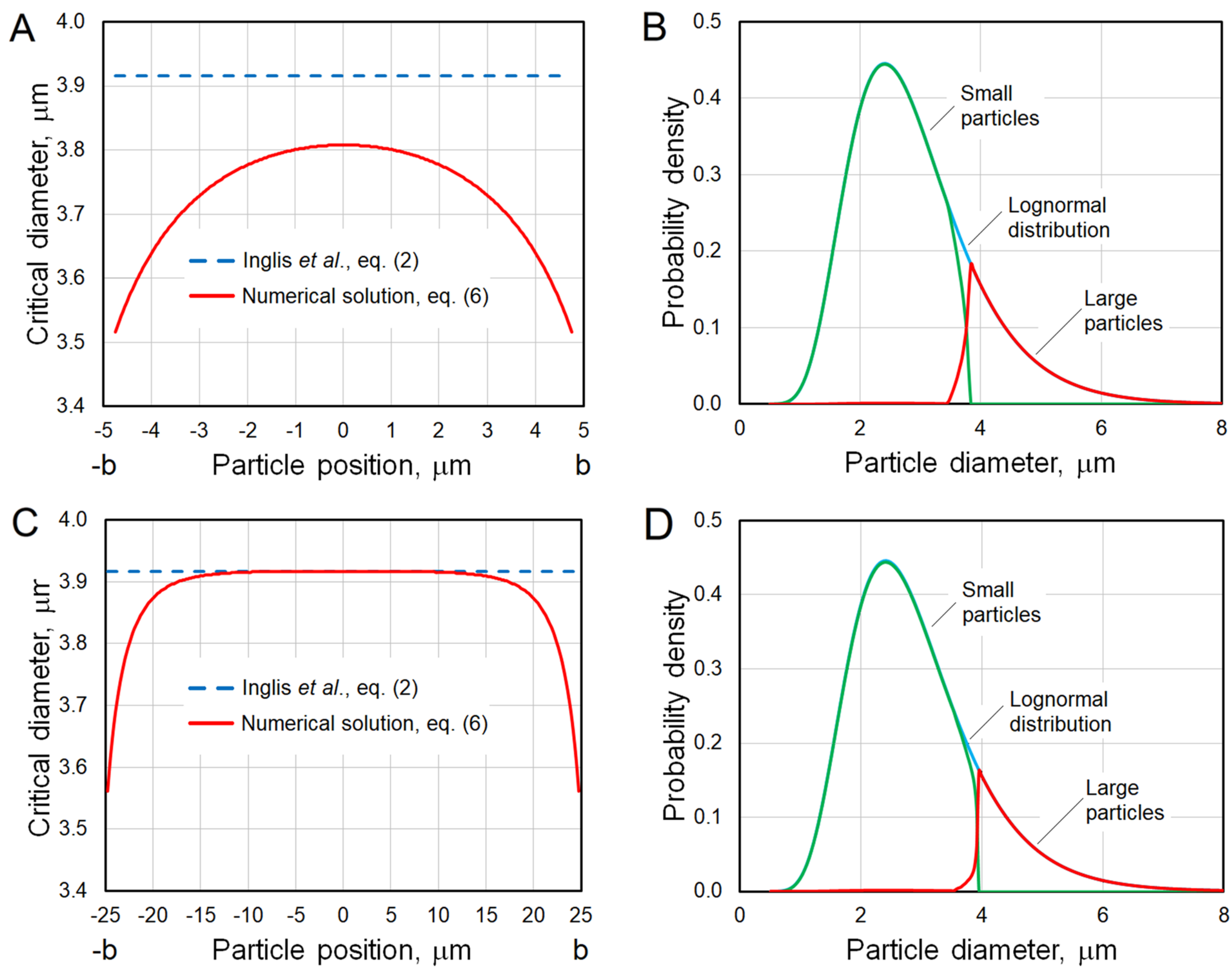

Fig. 4 Variation of critical diameter and efficiency of particle separation. The critical diameter versus the vertical position of particles in shallow **A** and deep **C** channels. Idealized separation of small and large particles in shallow **B** and deep **D** channels

Idealized particle separation

The previous subsection shows that the critical diameter depends on the position of the particle between the bottom and top of the channel. This means that in a real device, it is impossible to separate particles into strictly larger and strictly smaller ones than the given critical diameter.

Thus, if polydisperse particles are separated by a DLD, then after separation, the set of small particles will contain particles larger than the critical diameter, and vice versa, large particles will contain particles smaller than the critical diameter.

It was assumed that the diameter of polydisperse particles obeys the lognormal distribution:

$$f(x) = \frac{1}{x\sigma\sqrt{2\pi}} \exp\left(-\frac{(\ln x - \mu)^2}{2\sigma^2}\right) \quad (7)$$

where σ is the shape parameter (or the standard deviation of the log of the distribution) and μ is the scale parameter (or the median of the distribution). The shape and scale parameters affect the skewness of distribution. In the idealized case, shown in Fig. 4B and D, these parameters were chosen as $\sigma = 0.35$, and $\mu = 1$.

Figure 4B and D show the separation efficiency of the idealized DLD microfluidic devices with the geometric parameters described in the previous subsection. After separation, the probability density distributions of small and large particles were calculated numerically using the Eq. (6) for the critical diameter.

It can be seen that the separation boundary between small and large particles is not a sharp vertical line but is noticeably blurred. The separation efficiency increases with increasing channel height.

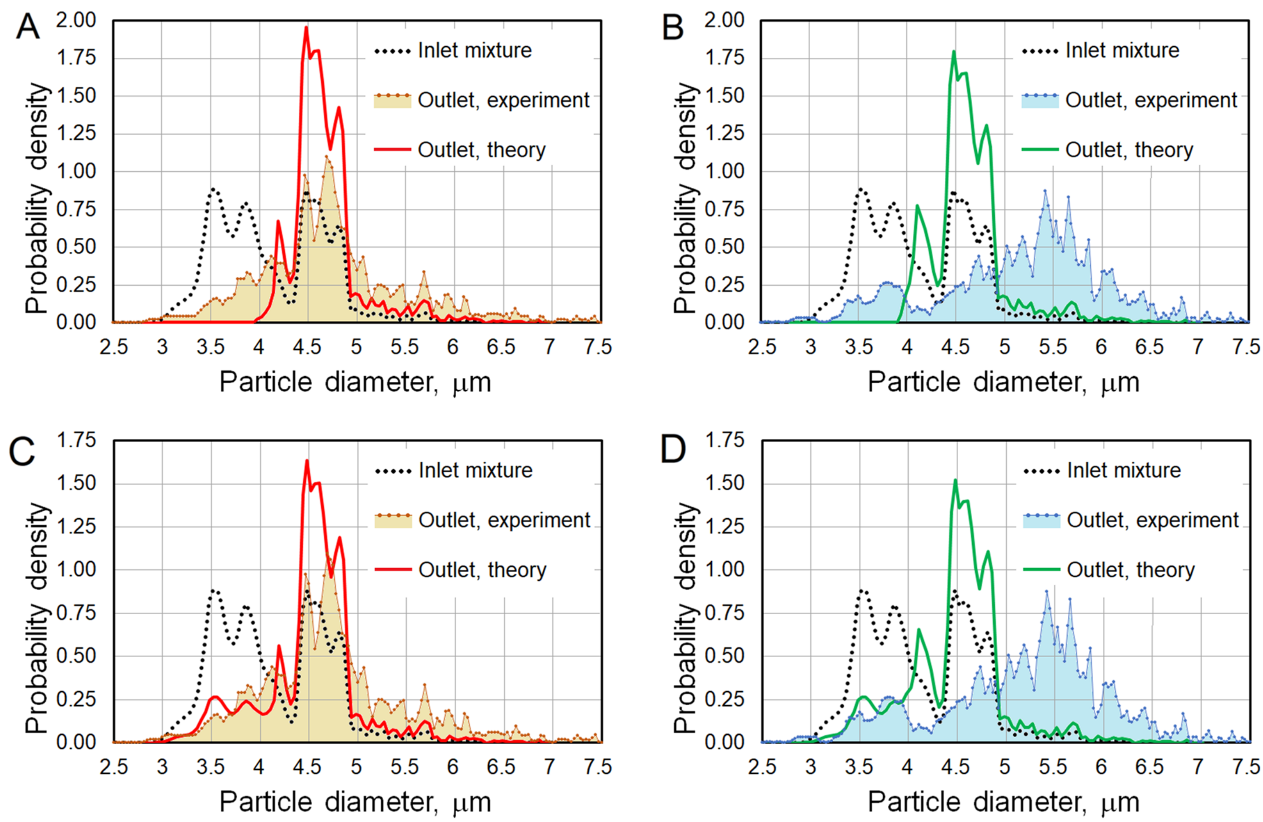

Fig. 5 Separation of particle mixture in deep (**A** and **C**) and shallow (**B** and **D**) channels. Idealized separation model in a deep **A** and shallow **B** channel, when separation efficiency is only affected by a change in the critical diameter. Realistic separation model in a deep **C** and shallow **D** channel, when 30% of the particles do not separate into large and small, reach the outlet and create noise in the particle size distribution

Experiment

The main goal of the experiment was to separate large particles from the polydisperse system, collect them at the outlet, and send small particles to waste. The idealized case was discussed in the previous section, and the separation results are shown in Fig. 4. The preliminary experiment results are shown in Fig. 5 and discussed below.

Preparation of polydisperse system

Three different sets of polystyrene particles purchased from Spherotech Inc (Lake Forest, IL) were mixed together: (1) particles with a diameter of 3.5 to 3.9 μm and a mean size of 3.80 μm; (2) particles with a diameter of 4.00 to 4.49 μm and a mean size of 4.16 μm; (3) particles with a diameter of 4.5 to 4.9 μm and a mean size of 4.79 μm. In all sets, the concentration of particles was 5% w/v. The aim was to obtain a mixture with an approximately uniform particle size distribution in the range of 3.5 to 4.9 μm. The final mixture contained particles with a minimum diameter of 2.1 μm and a maximum of 8.0 μm. The particle size distribution was measured using a cell counter (Z2 Coulter counter, Beckman Coulter) and is shown in Fig. 5 with black dotted lines.

Device design and fabrication

Two DLD channels were fabricated with the same gap ($g = 9$ μm) and row shift fraction ($\varepsilon = 0.1$), but at a different height (42.3 μm for the tall device and 10.8 μm for the shallow one).

The critical diameter calculated by analytical Eq. (2) is $D_c^{Inglis} = 3.52\ \mu m$. The critical diameter calculated by empirical Eq. (3) is $D_c^{Davis} = 4.17\ \mu m$. The ratio between these critical diameters is $D_c^{Davis}/D_c^{Inglis} = 1.185$. This ratio also visible in Fig. 2 at row shift fraction $\varepsilon = 0.1$.

The master mold of the microfluidic chip was fabricated by soft photolithography. A 4-inch Silicon wafer was spin-coated with negative photoresist (SU-8 2035, MicroChem, USA).

After spin coating, the wafer was soft-baked at 95 °C on a hot plate. The baked wafer was exposed to 160 mJ UV irradiation and baked (post-exposure bake) at 95 °C. After the baking, the wafer was developed using a developer (SU-8 developer, MicroChem, USA) and baked again (hard bake) at 150 °C. Hydrophobic surface treatment was then applied to the plate, finalizing the fabrication of the master mold. Finally, the polydimethylsiloxane (PDMS; Sylgard 184, Dow, USA) slab was fabricated using a conventional replica molding technique.

Outlet particle size distribution

Large particles were separated and collected at the outlet. The outlet particle size distribution was measured using a Z2 Coulter counter. The distribution at the outlet of the deep channel is shown by orange line with round markers in Fig. 5A and C. The distribution for the shallow channel is shown by a blue line with round markers in Fig. 5B and D.

Discussion

The inlet particle size distribution has four distinct peaks at 3.5, 3.85, 4.48, and 4.81 µm (see Fig. 5, black dotted lines). The output distribution shows that the 2.5 to 4.2 µm particles were mostly sent to waste. Thus, the critical diameter is higher than 4 µm, which is close to the $D_c^{Davis} = 4.17\ \mu m$. As shown above, the critical diameter reaches its maximum in the median plane between the top and bottom of the channel. Numerical calculations give a maximum critical diameter of 3.52 and 3.46 µm for deep and shallow channels, respectively, which is smaller than the Davis diameter [10] and corresponds to the Inglis diameter [2]. However, many publications have shown that the Davis diameter is more accurate than the Inglis diameter, and the Davis diameter is widely used to develop new devices [5–7]. For this reason, the results of numerical calculations of the critical diameter were multiplied by a factor of 1.18.

The numerically calculated size distributions of particles at the outlet of the deep and shallow channels are shown in Figs. 5A and B with red and green solid lines, respectively.

In this idealized case, the particle cut-off diameter is approximately 3.94–3.98 µm. In fact, the output particle size distribution contains the entire range of particle diameters, from the smallest to the largest. This is explained as follows. The particle concentration at the inlet is quite high. The flow rate between two adjacent posts and between the top and bottom of the channel varies from zero to the maximum value. Stagnation zones appear in the upper part of the posts where some streamlines terminate. Thus, the particles move with a large spread of velocities, and collisions are inevitable. In this way, small particles enter the outlet. As a result of numerical fitting, it was found that 30% of the particles reach the exit without separation into small and large ones and create noise in the particle size distribution at the outlet. Figure 5C shows a good agreement between the experimental data (orange line with round markers) and numerical calculation (red solid line) of DLD particle separation in the deep channel.

In the case of a shallow channel, the experimental data show a particle size distribution peak at 5.5 µm in the outlet reservoir (Fig. 5D, blue line with round markers). This means that most of the large particles in the range of 4.2 to 5.0 µm were sent to waste. The cross-section of the channel between the two posts is rectangular, 9 µm wide, and 10.8 µm high. The inlet mixture contains particles up to 8.0 µm in diameter. It is possible that a number of larger particles can be found. However, even two particles with a size of about 6.0–7.0 µm are enough to clog part of the channel. Blocking the microchannel with large particles disrupted the DLD separation. The larger cross-section in the deep channel (9 µm wide and 42.3 µm high) avoids blockage.

Thus, a deep channel allows less variation in the critical diameter across the height of the channel and provides better particle separation efficiency. A deep channel is less clogged than a shallow one. In addition, in the case of a deep channel, the hydraulic resistance is reduced, which makes it possible to increase the flow rate. However, high cylindrical posts in this case become very flexible, and their effect on the separation has not yet been studied.

Figure 1B shows that the device contains 10 posts in each row. The row shift fraction is $\varepsilon = 0.1$. This means that in 1 section of the device, all large particles will be deflected from the left to the right by one post. In "Theoretical analysis" Section, large particles will be deflected one more post to the right. Ideally, all large particles will be collected at the outlet after 10 sections. An increase in the number of sections, on the one hand, leads to an increase in the separation efficiency, and, on the other hand, can cause clogging of the microchannel. This issue requires further study.

Conclusion and further work

Theoretical analysis for the variation of critical particle diameter in deterministic lateral displacement separation has been presented, with additional parameters being the height of the microchannel and the level of particles between the top and bottom of the channel.

The analytical solution of the Poiseuille flow in a rectangular duct gives a more complete description of the critical diameter than the parabolic flow profile through the gap between two posts of the separation array.

Preliminary experiments show the effect of channel height on the critical diameter and efficiency of particle separation.

In further experiments, the gap between the posts should significantly exceed the size of the largest particles at the inlet. A wide range of experiments should be provided for different heights of the microchannel from the minimum, determined by the particle size, to the maximum, determined by the mechanical stability of the manufactured devices.

It is highly desirable that the particles in the initial mixture either obey a lognormal low or have a uniform distribution in the range of interest.

Acknowledgements
Not applicable.

Author contributions
JHB conducted the experimental part of the study. AZ carried out a theoretical analysis and wrote the manuscript. SY proposed the idea of the study, and reviewed/edited the manuscript. All authors read and approved the final manuscript.

Funding
This work was supported by the National Research Foundation of Korea(NRF) grant funded by the Korea government(MSIT). (No. NRF-2021R1A2C3008169).

Availability of data and materials
Not applicable.

Declarations

Ethics approval and consent to participate
Not applicable.

Competing interests
The authors declare that they have no competing interests.

Author details
[1]School of Mechanical Engineering, Gwangju Institute of Science and Technology (GIST), Gwangju 61005, Republic of Korea. [2]Department of Biomedical Science and Engineering, Gwangju Institute of Science and Technology (GIST), Gwangju 61005, Republic of Korea.

Received: 6 October 2022 Accepted: 21 November 2022
Published online: 30 November 2022

References

1. Huang LR, Cox EC, Austin RH, Sturm JC (2004) Continuous particle separation through deterministic lateral displacement. Science 304:987–990. https://doi.org/10.1126/science.1094567
2. Inglis DW, Davis JA, Austin RH, Sturm JC (2006) Critical particle size for fractionation by deterministic lateral displacement. Lab Chip 6:655–658. https://doi.org/10.1039/B515371A
3. Beech JP. Microfluidics separation and analysis of biological particles. Lund University: Lund. https://lup.lub.lu.se/record/2198801. 2011
4. Holm S. Microfluidic Cell and Particle Sorting using Deterministic Lateral Displacement. Department of Physics, Lund University, Lund. https://lup.lub.lu.se/record/bc57504b-5349-4a1a-8283-5eee9343c80e. 2018
5. McGrath J, Jimenez M, Bridle H (2014) Deterministic lateral displacement for particle separation: a review. Lab Chip 14:4139–4158. https://doi.org/10.1039/C4LC00939H
6. Salafi T, Zhang Y, Zhang Y (2019) A review on deterministic lateral displacement for particle separation and detection. Nano-Micro Lett 11:77. https://doi.org/10.1007/s40820-019-0308-7
7. Hochstetter A, Vernekar R, Austin RH, Becker H, Beech JP, Fedosov DA, Gompper G, Kim S-C, Smith JT, Stolovitzky G, Tegenfeldt JO, Wunsch BH, Zeming KK, Krüger T, Inglis DW (2020) Deterministic lateral displacement: challenges and perspectives. ACS Nano 14:10784–10795. https://doi.org/10.1021/acsnano.0c05186
8. Inglis DW (2009) Efficient microfluidic particle separation arrays. Appl Phys Lett. https://doi.org/10.1063/1.3068750
9. Al-Fandi M, Al-Rousan M, Jaradat MAK, Al-Ebbini L (2011) New design for the separation of microorganisms using microfluidic deterministic lateral displacement. Robot Comput-Integr Manuf 27:237–244. https://doi.org/10.1016/j.rcim.2010.06.003
10. Davis JA. Micro fluidic separation of blood components through deterministic lateral displacement. PhD thesis, Princeton University (2008)
11. White FM, Majdalani J. Viscous Fluid Flow, Fourth Edition, McGraw-Hill Companies, Inc.. 2022
12. Fukuchi T (2011) Numerical calculation of fully-developed laminar flows in arbitrary cross-sections using finite difference method. AIP Adv. https://doi.org/10.1063/1.3652881

Publisher's Note

Springer Nature remains neutral with regard to jurisdictional claims in published maps and institutional affiliations.

Submit your manuscript to a SpringerOpen journal and benefit from:

- ► Convenient online submission
- ► Rigorous peer review
- ► Open access: articles freely available online
- ► High visibility within the field
- ► Retaining the copyright to your article

Submit your next manuscript at ► springeropen.com